



A new view of coronal structures: implications for the source and acceleration of the solar wind

S. R. Habbal^{1*}, H. Morgan¹ and M. Druckmüller²

¹*Institute for Astronomy, University of Hawaii, 2680 Woodlawn Drive, Honolulu, HI, USA*

²*Brno University of Technology, Technická 2, 616 69 Brno, Czech Republic*

Abstract. We show how the complement of white light and a suite of Fe coronal forbidden line images taken during total solar eclipses since 2006 have yielded new insights into the physical properties of the coronal plasma and the role of the magnetic field. The unique properties of these spectral lines make them ideal diagnostic tools for exploring the first few solar radii above the photosphere where the expansion of the corona and the acceleration of the solar wind occur. In particular, these observations show how: (1) localized enhancements of the ion densities relative to electrons appear in some magnetic structures, (2) the transition between a collision-dominated to a collisionless plasma occurs within a heliocentric distance of 1.2 - 1.6 R_s , (3) the expanding corona is characterized by an electron temperature of 10^6 K, and (4) prominences are enshrouded by hot 2×10^6 K coronal plasma. We discuss the implications of these observations for the source and acceleration of the solar wind.

Keywords : Sun: corona – solar wind – eclipses

1. Introduction

The advent of white light and ultraviolet observations from SOHO, namely the C2 coronagraph on LASCO (see Brueckner et al. 1995), and UVCS (see Kohl et al. 1995), significantly enhanced our empirical capabilities for probing the acceleration region of the solar wind. These were the first observations of the corona, outside of total solar eclipses, to span heliocentric distances (the distance standard used throughout this paper) exceeding 2 solar radii (R_s). These observations showed that heavy ions are probes of the processes that accelerate the solar wind. Most notable among these

*email: shadia@ifahawaii.edu

discoveries were the very high ionic temperatures exceeding 10^8 K in the fast solar wind, with speeds larger than the bulk proton-electron solar wind speed below $10 R_s$ (e.g. Li et al. 1998, Kohl et al. 1998). The white light LASCO images provided new views of coronal structure and yielded an unexpectedly rich variety of coronal mass ejections (CMEs) (St. Cyr et al. 2000). Missing from these space-based coronagraph observations, however, was information from the coronal region obscured by the occulters, and hence the link to the Sun. Although EUV images of the corona cover the solar disk and the corona, and can, in principle, fill the coronagraph gap, they are limited in their diagnostic capabilities to $1.25 R_s$, because of the sharp decrease of the intensity of the EUV lines with distance.

Ironically, at present, eclipse observations remain the only opportunities to adequately fill the distance range of $1 - 3 R_s$. Despite their short durations and the whims of ground-based observing conditions, we show in this review how recent eclipse observations, which capitalized on the diagnostic properties of the coronal forbidden lines, not only filled this important gap, but also yielded novel results regarding the behavior of heavy ions. They led to new insights into the range of observed scales in coronal structures and into the thermodynamic properties of the corona where the magnetic field undergoes the most dramatic expansion and the solar wind is accelerated.

2. Large scale coronal structures

Shown in Fig. 1 is a white light image of the corona taken during the total solar eclipse of 2010 July 11. The image has been processed by the Adaptive Circular High-pass Filter, or ACHF, developed by M. Druckmüller, Rušin & Minarovjech (2006) to reveal the finest details of coronal structures at the 1 arcsec limit of the spatial resolution of the data. Most striking in this image is the bewildering variety of density structures, which are assumed to trace the magnetic field lines in the corona. The solid and dashed lines overlaid on the image trace some outstanding features. There is a preponderance of small scale loop-like structures, labeled *l* all around the Sun with the exception of the polar regions. These are in contrast to the large-scale loops labeled *L*. *SB* and *SS* refer to a streamer boundary and streamer stalk, respectively. The *Ray* is a seemingly lone field line that seems to cross other structures. The *Hook* is the envelope of a prominence that erupted a few hours prior to the eclipse. The *Ripple*, *Streak* and *Cone* pertain to large scale disturbances created by the passage of two CMEs through the corona prior to the eclipse observations. *WSB* refers to a wavy streamer boundary also created by the passage of the CME in the southwest. *E* refers to some enhancement produced by the projection of material from the bulge of a streamer along the line of sight, most likely in the foreground since it is very pronounced. The red structure off the limb towards the south-west is a large-scale prominence emitting strongly in $H\alpha$, within the bandpass of the white light. Filling the field of view is a plethora of open field lines originating from all latitudes around the solar disk. These are described in more detail in Habbal et al. (2011).

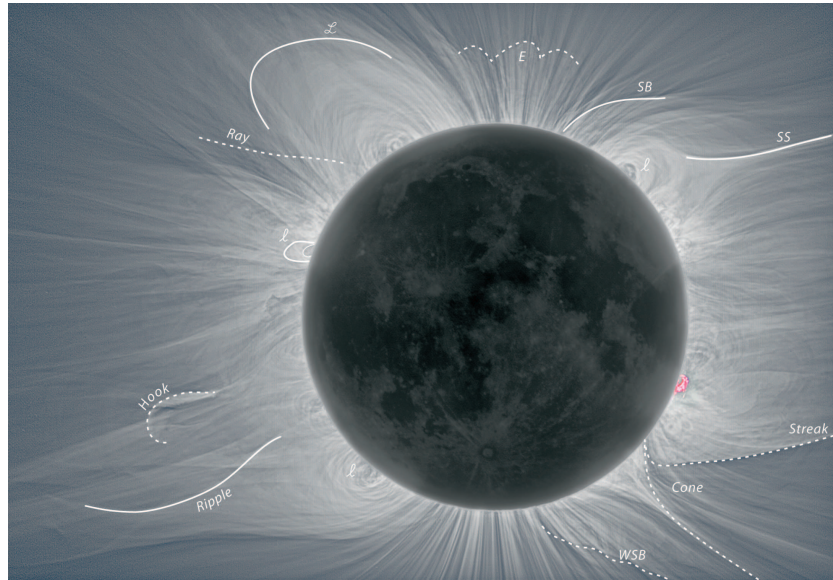


Figure 1. White light image of the corona taken by M. Druckmüller during the total solar eclipse of 2010 July 11. The image has been processed with the ACHF to bring out the small scale structures in the corona. The line traces in solid and dash refer to distinct and uncommon structures in the corona. (See Habbal et al. 2011 for details.)

White light images, which serve as a proxy for the magnetic field lines, however, reflect only the distribution of electron densities along the line of sight. Imaging in emission from ions covering a range of peak ionization temperatures, complements the white light by yielding the distribution of ion densities and electron temperatures along the line of sight. The suite of Fe coronal forbidden lines, namely Fe IX 435.9 nm, Fe X 637.4 nm, Fe XI 789.2 nm, Fe XIII 1074.7 nm, and Fe XIV 530.3 nm, covers the temperature range of $0.8 - 2 \times 10^6$ K. Shown in Fig. 2 are overlays of Fe XI, Fe XIV and white light taken during the eclipses of 2008, 2009 and 2010, with Fe XI only in 2006. Fe XI has a peak ionization temperature of 1.18×10^6 K, and Fe XIV of 2×10^6 K. Such composites associate coronal structures with distinct temperatures. From these three years of observations, it is clear that the extended corona, i.e. comprising open field lines, is dominated by the cooler Fe XI emission, while the bulges of the streamers consist primarily of hot plasma emitting in Fe XIV.

Shown in Fig. 3 is the northwest quadrant of the 2008 eclipse image from Fig. 2a where a large prominence, as seen in the red $H\alpha$ emission (panel b), was present. The close-up views on the right (panels c) were produced with another image processing tool, the Normalizing Radially Graded Filter, NRGF, developed by Morgan et al. (2006). They include observations from Fe X, Fe XI, Fe XIII and Fe XIV taken at the same time. The line plots in panels e are the spectral line intensities as a function of position angle at different heights. It is clear from the spectral lines (panels

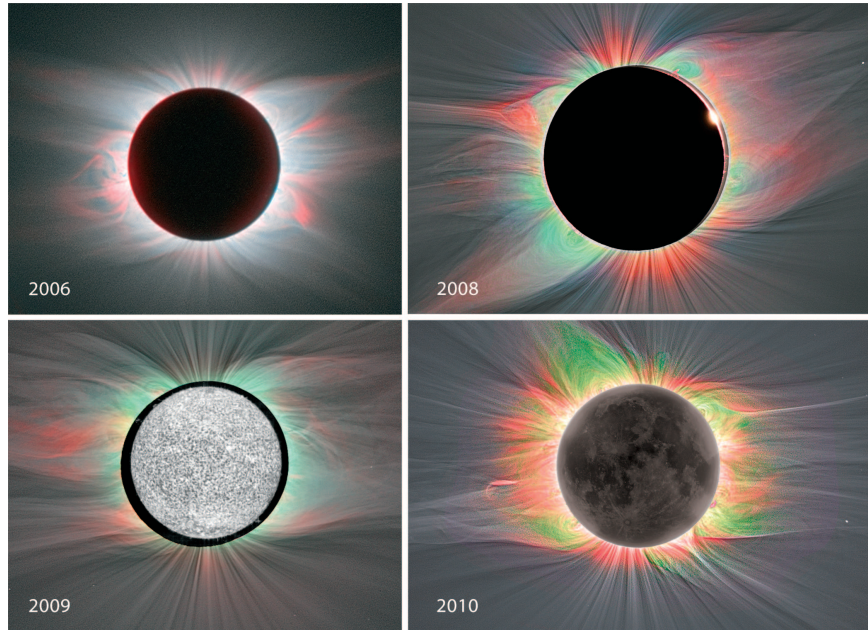


Figure 2. Overlay of white light, Fe XI 789.2 nm (red) and Fe XIV 530.3 nm (green) ACHF-processed images, from the 2008, 2009 and 2010 eclipses observations. He II 30.4 nm SOHO/EIT disk emission is shown for 2009 only. In 2006, only Fe XI with white light was available.

c), and their overlay with white light (panel a), that the prominence is surrounded by the hottest coronal material, as is also evident in the line plots (panels e) where a peak in the intensity of Fe XIII and Fe XIV corresponds to a dip in the Fe X and Fe XI emission. These multi-wavelength observations thus show that prominences, the coolest and most complex magnetic structures suspended in the corona (see Tandberg-Hanssen 1995), are enshrouded in hot plasmas of twisted magnetic structures, commonly known as 'coronal cavities', which form the bulges of streamers and are so named due to their dark appearance in white light images. The density within a cavity is often low compared to surrounding structures. However, as shown in Fig. 3 the material that is present is hot for reasons currently unknown.

3. Physics of the solar corona

One striking feature in the overlays in Fig. 2 is the extent of the emission from the Fe lines, which is unexpected if one considers images from their EUV counterparts where the emission cuts off beyond approximately $0.25 R_s$. The extent of the emission can be accounted for by considering the two main processes that contribute to the intensity I_λ of a given spectral line λ , namely: (1) collisional excitation, I_C , and (2) radiative

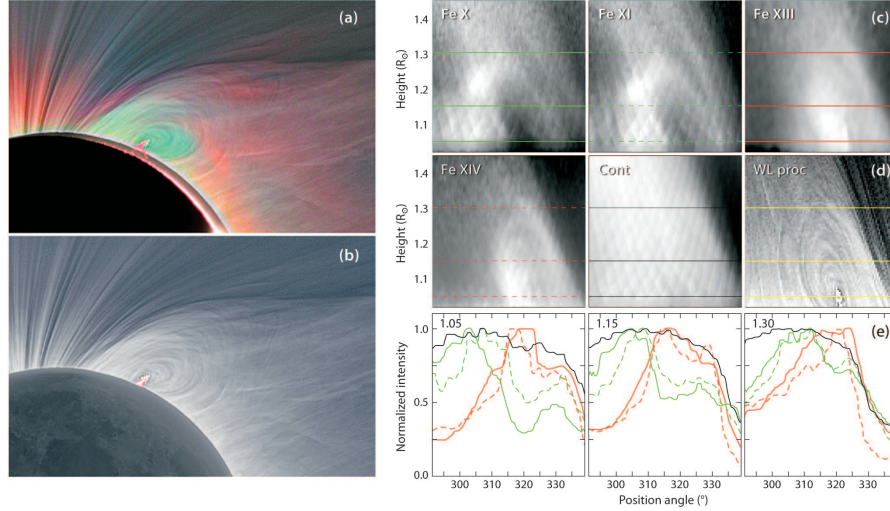


Figure 3. Fe XI/Fe XIV/White light composite (a) and white light (b) of the northwest quadrant of the 2008 eclipse field of view. Rows (c) and (d): Close-up views of Fe X, Fe XI, Fe XIII, Fe XIV, and 787.86 nm continuum emission processed with NRGF, and broad-band white light with ACHF. The horizontal dashed lines correspond to the distances where the normalized emission line intensities are plotted in (e) below. Row (e): Spectral line intensities normalized to their corresponding maximum value (y-axis) versus position angle (x-axis), at 1.05, 1.15 and 1.3 R_s with Fe X (green), Fe XIII (red), Fe XIV (dashed-red), 787.86 nm continuum (black). [From Habbal et al. (2010c).]

excitation, I_R . To first approximation this can be simply written as:

$$I_\lambda = I_C + I_R \approx \int A N_e N_i ds + \int B N_i ds \quad (1)$$

where N_i is the ion density, N_e the electron density, A and B are coefficients including atomic data and incident disk radiation. The integration is along the line of sight over a distance s . It is clear that very close to the Sun when the first term is dominant, the intensity drops sharply because of the density squared dependence. Once this contribution diminishes significantly, the radiative component (second term), produced by the excitation and subsequent spontaneous de-excitation of coronal ions by light from the solar disk, is still present. It is precisely this contribution that enables the emission to persist much further away from the Sun than emission from EUV lines for which only the collisional component (first term) exists.

The continuum, or white light, on the other hand, is due to scattering of the photospheric radiation by free coronal electrons. It can also be given in very simple terms by:

$$I_{WL} \approx \int C N_e ds \quad (2)$$

where C includes the photospheric radiation and geometrical factors. Both the white light (Eqn. 2) and the radiative term I_R in Eqn. 1 are very similar in that they are both proportional to the line of sight integration of the product of density and the incident disk radiation. Because of its linear dependence on density, the white light emission can be detected to large distances, as demonstrated by numerous eclipse observations (e.g. Fig. 1) and by the coronagraph images from LASCO/C2 and C3, as well as STEREO.

Taking the ratio of the intensity of line to continuum using Eqns. 1 and 2 gives, to first approximation:

$$\frac{I_\lambda}{I_{WL}} \approx \frac{A}{C} N_i + \frac{B}{C} \frac{N_i}{N_e} \quad (3)$$

which leads to some interesting insights. The first term is dominant when collisions are still important, and should decrease sharply with distance. The second term persists when radiative excitation becomes the dominant process. It should be flat if both ion and electron densities decrease in the same manner with distance.

An example of the validity of this simple concept is shown in Fig. 4a,b for two sections of the 2006 eclipse image processed with the NRGF. We note that the NRGF reveals the presence of enhanced Fe XI intensities in different regions of the corona. The traces shown in the plots were calculated along different paths starting from the solar surface outwards. In the example of panel b, the transition from a collision-dominated excitation to a radiatively-dominated excitation is determined by the sharp change in slope of the ratio, namely from a steep drop to a flattening, as expected from Eqn. 3. In panel a, the peak in the ratio corresponds to the localized enhancements in the Fe XI emission, which then translates into an enhancement of the ion relative to the electron density, as seen from the second term in Eqn. 3. Given that such a transition from collisional to radiatively-excited emission can actually be determined empirically, one can then apply this technique to define the locus of this transition, R_t , in the two-dimensional image, as shown in panels c for the 2008 eclipse. We note that R_t , which ranges between 1.1 and 2 R_s , is a function of the underlying coronal structures and their corresponding temperature. As is apparent from the ratio of line to continuum in Fig. 4, the slope of the ratio decreases and becomes flat over a short distance range, therefore R_t is not really an abrupt boundary but should rather be considered as a transition zone spanning approximately 0.1 R_s .

By definition, R_t also determines the locus of the departure of the plasma from ionization equilibrium as the plasma flows into low-density regions (Habbal et al. 2010a,c). Hence R_t effectively represents an important empirical threshold. For distances smaller than R_t , the plasma is dominated by collisions, hence it is meaningful to consider a plasma electron temperature. Indeed a unique feature of the superposition of images from different wavelengths, as shown in the example of Fig. 2, is that it yields a two-dimensional map of the electron temperature in the context of density/magnetic structures. With these maps, the 2006 - 2009 eclipse observations

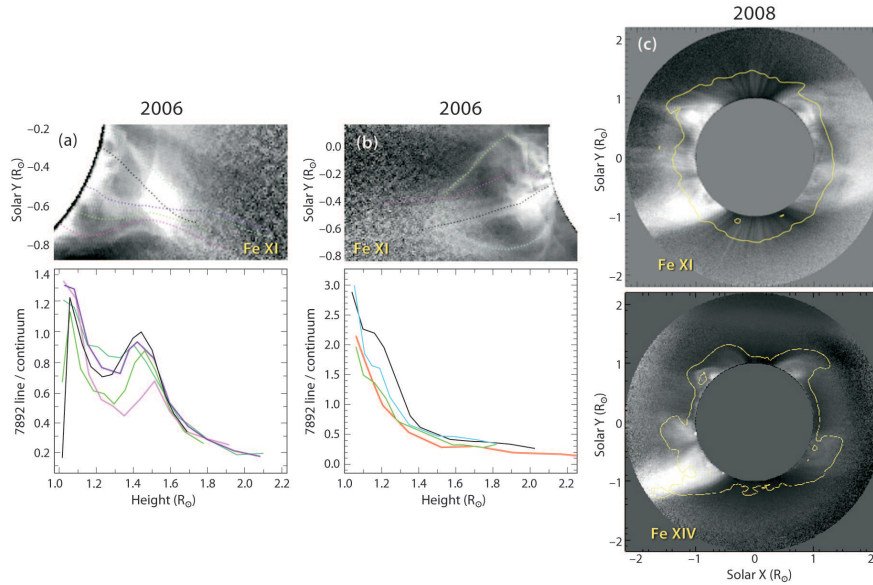


Figure 4. Columns (a) and (b) are sections of the NRGF-processed Fe XI 789.2 nm 2006 eclipse image where evidences of ion density enhancements were observed (see Habbal et al. 2007a). The ratio of line to continuum intensities is given in the plots for the different traces shown in the corresponding images above them. The localised enhancements in (a) are visible in the ratio for all traces. The flattening of the ratio around 1.5 R_s in (b) indicates the locus of the transition, R_t, to a predominantly radiatively excited emission. In (c), the contours of R_t are overlaid over the NRGF-processed 2008 Fe XI and Fe XIV eclipse images.

indicate that the open field lines in the corona are characterized by cooler electron temperatures averaging 10^6 K (Habbal et al. 2010a).

Beyond R_t where the plasma is practically collisionless, the emission then reflects the distribution of the corresponding charge state. In the examples of 2006 - 2009, the emission was dominated by Fe XI, implying the dominance of Fe⁺¹⁰ charge state in the expanding corona. One relevant comparison is with in situ Fe⁺ⁿ charge state measurements, with the most comprehensive one being the full solar cycle sequence from 1998 to 2009 from the SWICS instrument on ACE. Shown in Fig. 5 is the calculated distribution of the electron temperature that best reproduces the ACE data (see details in Habbal et al. 2010b). It is found that the peak of the distribution is at 1.18×10^6 K, which matches remarkably well the peak ionization temperature of Fe XI. Hence, the in situ measurements are a direct reflection of the distribution of Fe charge states in the corona, which is reflected in the dominant emission beyond R_t as shown in the example of Fig. 4. The persistence of this trend throughout the solar cycle is therefore quite remarkable.

4. Discussion and conclusions

At present, models remain the only tool to explore the physical processes that heat the corona and drive and accelerate the solar wind. Prior to the SOHO era, in situ measurements of solar wind plasma parameters, such as composition (e.g. von Steiger et al. 2000), density, temperature and speed of the solar wind species (e.g. Marsch 1987) were the only data available to guide the development of single- and multi-fluid solar wind models. In the inner corona, plasma properties were limited to the electron density inferred from polarized white light measurements, and electron temperature derived from the ratio of the intensities of some EUV lines (e.g. Habbal et al. 1993). With the advent of SOHO, new empirical constraints became available, confirming some model results (e.g. Habbal et al. 1995, Li et al. 1997), and steering them in new directions (e.g. Esser and Edgar 2000). The most significant impact (e.g. Li et al. 1998) came from observations of emission from heavy ions in the extended corona, i.e. out to $10 R_s$, primarily from $Ly\alpha$ and the O VI doublet lines at 103.2 and 103.7 nm with UVCS, as originally proposed by Noci et al. (1987). Inferences of the outflow velocity of protons and heavy ions, together with the ion temperature in the inner corona were possible for the first time. Also feasible for the first time were inferences of the true 3D structure of the corona, as observations were routinely made with high spatial and temporal resolution. These were accomplished by tomography (Morgan and Habbal 2010) or by other empirical methods (Morgan & Habbal 2007a,b).

This review has focused on recent eclipse observations, starting from 2006, because of the new insights they have provided, enhancing and complementing the recent findings from SOHO, STEREO and SDO. The eclipse observations also underline the increased importance of exploring the behavior of heavy ions. The diagnostic potential of these observations became possible with the advent of new imaging technology and the development of reliable image processing tools. The suite of Fe lines, such as the Fe X, Fe XIII and Fe XIV lines, which had been extensively observed in the past, was enhanced by the more recently exploited Fe XI line, when the corona was imaged in this line for the first time in 2006 (Habbal et al. 2007a). Not only was a series of lines from the same element with increasing ionization temperature readily available for exploration, it was also realized that these lines had something special to offer due to the importance of their radiatively excited component. This component enables their emission to be observed out to large distances from the Sun, much further than their EUV counterparts. These observations thus led to the following novel results:

The extent of the emission from the coronal forbidden lines, starting from the solar surface out to a few solar radii, provides the only observational evidence for the range of spatial scales of closed field lines in the corona, the evolution of density structures commonly referred to as streamers, and the distribution of open field lines throughout the corona which is clearly not limited to the polar regions. Hence the solar wind flow cannot be limited to coronal holes. However, since these observations do not have velocity diagnostics, they cannot provide the characteristics of the outflows

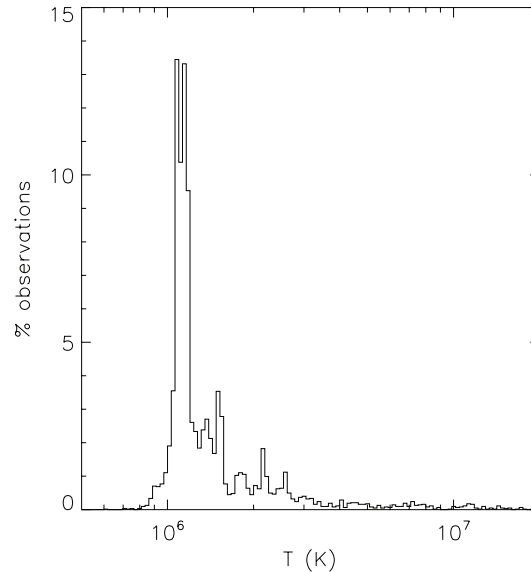


Figure 5. Calculated distribution of T_e that best reproduces the 12 hour averages of the SWICS/ACE Fe^{n+} (with $n = 6$ to 20) charge state measurements from 1998 to 2009. The vertical axis is the percent of observations in each temperature bin. The peak of the distribution is at 1.18×10^6 K, which matches remarkably well the peak ionization temperature of Fe XI.

along all open field lines. The extent of the emission also enabled, for the first time, the empirical determination of the location, R_l , where the emission from each of these spectral lines transitions from being dominated by collisions to being dominated by radiative excitation. This is also the locus where the plasma is no longer dominated by collisions.

These observations also yielded the first 2D distribution of the electron temperature and Fe charge states in the corona. They clearly tagged the closed versus open magnetic field lines with distinct temperatures, a distinction that was not possible with earlier observations. They yielded the surprising result that open field lines are unequivocally dominated by plasma with an electron temperature of 10^6 K, in contrast to the wide range of values inferred from earlier studies (see e.g. Habbal et al. 1993). This new result is consistent with the dominance of the Fe^{+10} charge state in the corona that matches remarkably well in situ charge state measurements over a full solar cycle. This electron temperature also emerges from solar wind models incorporating radiative losses and thermal conduction (e.g. Lie-Svendson & Esser 2005).

One of the surprising discoveries to emerge from these observations was the existence of magnetic configurations conducive to the formation of localized ion density enhancements relative to that of electrons, also referred to as abundances. Such en-

hancements had been found earlier in model studies (e.g. Lie-Svendson and Esser 2005). This phenomenon, which places several useful constraints on models, was observed for the first time in the eclipse data. Indeed, the imaging of the corona in the visible and near infrared (NIR) emission lines was the perfect observation to discover such a phenomenon, since the intensity of the emission line could be directly compared to the neighboring continuum, made with an identical observing system. Once identified in the eclipse data, they can be shown to be present in EUV images (Habbal 2007a). The recent study by Byhring et al. (2011) was able to reproduce the 2006 Fe XI observations of abundance enhancements in a slow solar wind flow by reducing the heat input to heavy ions, thus leading to their decoupling from the protons, and consequently lagging behind in the corona.

The eclipse observations also provide ample evidence of the intricate behavior of the large scale density structures in response to the eruption of filaments or the passage of CMEs. This behavior is further tagged with well-defined temperature characteristics. Furthermore, the observed twisted helical structures associated with prominences within the bulges of streamers (see also Fig. 1) provide the most direct evidence for the emergence of helicity with prominences that is not limited to the prominences themselves, but extends to their immediate surroundings. The existence of the complex of prominence surrounded by a hot shroud should have implications for coronal heating mechanisms in the neighborhood of magnetic polarity reversal regions.

In conclusion, eclipse observations continue to provide unique opportunities for exploring the physics of the corona. The recent discoveries summarized here should have an impact on future modeling efforts. Hopefully, they will also inspire a new generation of space-based coronagraphs with the ability to image the corona in visible and NIR emission lines. Such observations would provide the constraints that increasingly sophisticated coronal models need.

Acknowledgements

The eclipse observations described here were made possible thanks to the outstanding efforts of Judd Johnson, together with unselfish support from members of the eclipse team, *the Solar Wind Sherpas*. Funding for this work was provided by NASA grants NNX08AQ29G and NNX07AH90G, and NSF grant ATM 08-02520 to the University of Hawaii, Institute for Astronomy. Partial support for the work of M. Druckmüller was provided by grant 205/09/1469 of the Czech Science Foundation. We thank Karen Teramura for her artistic preparation of the figures.

References

- Brueckner G. E., et al., 1995, *Sol. Phys.* 162, 357,
Byhring H. S., Cranmer S. R., Lie-Svendson Ø., Habbal S. R., Esser R., 2011, *ApJ*, 732, 119

- Druckmüller M., 2009, *ApJ*, 706, 1605
- Druckmüller M., Rušin V., Minarovjech M., 2006, *Contributions of the Astronomical Observatory Skalnaté Pleso*, 36, 131
- Esser R., Edgar R. J., 2000, *ApJ*, 532, L71
- Habbal S. R., Esser R., Arndt M., 1993, *ApJ*, 413, 435
- Habbal S. R., Esser R., Guhathakurta M., Fisher R., 1995, *Geophys. Res. Lett.*, 22, 1465
- Habbal S. R., et al., 2007a, *ApJ*, 663, 598
- Habbal S. R., et al., 2007b, *ApJ*, 670, 1521
- Habbal S. R., et al., 2010a, *ApJ*, 708, 1650
- Habbal S. R., Morgan H., Druckmüller M., & Ding A., 2010b, *ApJ*, 711, L75
- Habbal S. R., et al., 2010c, *ApJ*, 719, 1362
- Habbal S. R., et al., 2011, *ApJ*, 734, 120
- Kohl J. L., et al., 1995, *Solar Phys.*, 162, 313
- Kohl J. L., et al., 1998, *ApJ*, 501, L127
- Lie-Svendsen Ø., Esser R., 2005, *ApJ*, 618, 1057
- Li X., Esser R., Habbal S. R., Hu Y. Q., 1997, *J. Geophys. Res.*, 102, 17419
- Li X. et al., 1998, *ApJ*, 501, L133
- Marsch E., 1987, in *Physics of the Inner Heliosphere*, p. 45, R. Schwenn and E. Marsch (Eds.), Springer-Verlag
- Morgan H., Habbal S. R., Woo R., 2006, *Solar Phys.*, 236, 263
- Morgan H., Habbal S. R., 2007a, *A&A*, 464, 357
- Morgan H., Habbal S. R., 2007b, *A&A*, 465, L47
- Morgan H., & Habbal S. R., 2010, *ApJ*, 710, 1
- Noci G., Kohl J. L., Withbroe G. L., 1987, *ApJ*, 315, 706
- St. Cyr O.C., et al., 2000, *J. Geophys. Res.* 105, 18169
- Tandberg-Hanssen E., 1995, *The Nature of Solar Prominences*, Kluwer Academic Publishers
- von Steiger R., et al., 2000, *J. Geophys. Res.*, 105, 27217